Monte Carlo Simulation of Rarefied Flow Along a Flat Plate

W. L. Hermina*
Sandia National Laboratories, Livermore, California

The direct simulation Monte Carlo technique is applied to a diverging flowfield along a flat plate. The model accounts for a plate of finite thickness with a nonzero leading edge bevel angle, and permits the specification of surface accommodation coefficients ranging from diffuse to specular reflection. The computed density, velocity, and temperature profiles at several axial stations along the plate are compared with experimental data. These comparisons indicate good agreement when the leading edge bevel is included in the calculation, and when the surface accommodation coefficients are each assigned a value of 0.8. Results are also presented that indicate the sensitivity of the computed skin friction to the ratio of the computational cell size to molecular mean free path. The results indicate that the skin friction is insensitive to the cell size if the local Knudsen number based on the cell size is maintained larger than unity everywhere in the flowfield. The results also indicate that the skin friction is underpredicted toward the plate leading edge and overpredicted at downstream axial positions when the cell size exceeds the molecular mean free path.

Nomenclature

C_f	= skin friction
h	= plate thickness
Kn_c	= local Knudsen number based on transverse cell size, $\lambda/\Delta y$
Kn_L	= local Knudsen number based on plate length, λ/L
$Kn_{\infty,c}$	= freestream Knudsen number based on the transverse cell size, $\lambda_\infty/\Delta y$
$Kn_{\infty,L}$	= freestream Knudsen number based on the plate length, λ_∞/L
L	= plate length
M	= Mach number
T	= temperature
u	= axial velocity component
v	= transverse velocity component
x	= axial position relative to line source
y	= transverse position above plate surface
β	= plate leading edge bevel angle
γ	= ratio of specific heats
λ	= mean free path
ρ	= gas density
σ	= molecular collision cross section
ω	= temperature exponent for elastic collision cross section

Subscript

∞	= freestream value at plate leading edge

Introduction

THE direct simulation Monte Carlo technique[1] is used to model gas dynamics along a flat plate exposed to an expanding freejet. This flowfield has been chosen because of the availability of spatially resolved measurements[2] of gas density, velocity, and temperature for comparison with computations. Previous comparisons[3] have been limited to surface drag as a result of limited availability of such flowfield data. In addition to the above comparisons, the sensitivity of the computed results to the ratio of the mean free path to cell size is also discussed.

Many of the features incorporated in the present Monte Carlo capability have been described previously elsewhere.[3-5] The capabilities, however, have been extended to permit the treatment of two-dimensional diverging incoming flows, as is needed for this special flow situation. The divergence angle is chosen to match measured flow conditions, as described below. The ability to simulate a finite plate thickness with a nonzero bevel angle is also included. In addition, the variable-hard-sphere (VHS) collision model developed by Bird[6] has been included in the collision algorithm to permit a more rigorous treatment of the collision dynamics. The necessary parameters for the VHS model are based on experimental measurements[7] of the gas viscosity as a function of temperature over the temperature range of interest for the flowfield.

Computational Techniques

The flowfield emanating from a freejet is an axisymmetric expansion. The positioning of a flat plate within the flowfield results in a three-dimensional flowfield. For the present work the plate is assumed to be positioned along the freejet centerline and the gas expansion, both normal and transverse to the plate surface, is simulated by a two-dimensional flow with an effective expansion normal to the surface, as indicated in Fig. 1. Since the spanwise expansion is neglected, there are no spanwise gradients.

With this two-dimensional flowfield assumption, expanding flow is assumed to emanate from a line source far upstream of the plate. The flow expansion angle is constant, resulting in an inverse linear dependence of the density on axial position, as indicated by Eq. (1). An axisymmetric freejet expansion would result in an inverse quadratic dependence of density on axial position. However, this quadratic dependence can be approximated locally by a linear dependence that matches the measured density gradient along the plate.

$$\rho(x_1)x_1 = \rho(x_2)x_2 \tag{1}$$

The data presented in Ref. 2 indicate the axial Mach number gradient. This can be related to an axial density gradient by using the isentropic expression indicated by Eq. (2). The resulting density gradient can then be used in conjunction with Eq. (1) to determine the axial distance between the line source and plate leading edge required to match the measured axial Mach number gradient.

Received June 4, 1987; presented as Paper 87-1547 at the AIAA Thermophysics Conference, Honolulu, HI, June 8-10, 1987; revision received Nov. 9, 1987.

*Member, Technical Staff, Computational Mechanics Division. Member AIAA.

$$\frac{\rho(x_1)}{\rho(x_2)} = \left\{\frac{1+[(\gamma-1)/2]M^2(x_2)}{1+[(\gamma-1)/2]M^2(x_1)}\right\}^{1/(\gamma-1)} \tag{2}$$

The mean velocity components of the incoming molecules are then given by Eqs. (3) and (4), where x represents the axial distance between the line source and the upstream boundary of the computational domain (see Table 2), and y represents the transverse position above the plate surface. In addition, the flow divergence angle is assumed to be small such that $\cos(\theta) \sim 1$. The velocity components of individual incoming molecules are then determined by combining the mean velocity components with the thermal components determined from a Boltzmann distribution at the freestream temperature.

$$u = u_\infty \tag{3}$$

$$v = u_\infty\left(\frac{y}{x}\right) \tag{4}$$

To permit the accurate treatment of leading edge effects, the model treats a plate of finite thickness with a specified bevel angle, as indicated in Fig. 1. This effect is simply included by simulating the leading edge bevel as an additional surface connected to the leading edge of the plate and inclined by the bevel angle. The leading edge bluntness is neglected.

The calculations were performed on a rectangular mesh above the plate, and a modified rectangular mesh below the plate, as indicated in Fig. 1. The computational cells below the plate surface and just upstream of the bevel are truncated by the leading edge bevel. The computational mesh above the plate consists of 60 axial divisions and 40 transverse divisions for a domain 60 mm in length and 20 mm in height. This results in a cell size 1 mm in length and 0.5 mm in height. As will be indicated in a later section, this transverse cell size is a fraction of the local mean free path throughout the flowfield. In addition to this high resolution mesh, coarser meshes were used to study the sensitivity of the computed flowfield to the cell size. For these other cases, the transverse cell size was increased by as much as a factor of 20, giving a transverse cell size approximately eight times larger than the freestream mean free path.

To examine the sensitivity of these results to the downstream boundary conditions two different boundary flux models were tried: first, an outflow boundary, and second, a zero streamwise gradient technique, described by Vogenitz et al.[8]

A general surface accommodation model is included that permits the independent specification of the accommodation coefficients for the translational energy, rotational energy, and scattering angle. However, because the test gas used here (helium) has no rotational energy, only the accommodation coefficients for the translational energy and scattering angle are specified. Each accommodation coefficient represents the probability that the corresponding molecular degree of freedom will equilibrate with the surface upon collision. Consequently, for a scattering accommodation coefficient less than unity, some molecules will be specularly reflected. Similarly, for an energy accommodation coefficient less than unity, some molecules will not exchange energy with the surface.

To permit the accurate simulation of the flow structure, the variable hard sphere (VHS) collision model[6] is used. This permits treatment of the collision energy dependence of the elastic collision cross section. The functional form of the VHS collision model, giving by Eq. (5), was fit to values of the hard sphere collision cross section that are based on measured viscosity data.[7] The resulting values for the reference cross section σ_{ref}, the reference temperature T_{ref}, and the collision ω, are indicated in Table 1. These values reproduce the measured cross sections to three significant digits over a temperature range from 15 to 290 K, which encompasses the temperatures of interest for these calculations.

$$\sigma = \sigma_{ref}(T_{ref}/T)^{\omega} \tag{5}$$

Table 1 Variable hard sphere model parameters

σ_{ref}	1.452×10^{-19} m^2
T_{ref}	273.0 K
ω	0.149

Table 2 Plate description

Length	51 mm
Thickness	6 mm
Leading edge bevel angle	20 deg
Line source to leading edge distance	65.8 mm
Distance from line source to beginning of domain (x)	60.8 mm
Plate temperature	290 K

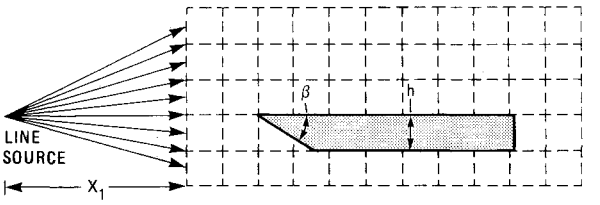

Fig. 1 Computational configuration for calculations.

Table 3 Freestream conditions at leading edge

Stagnation temperature	296 K
Temperature	11.3 K
Density	1.51×10^{-5} kg/m^3
Pressure	$3.8\ 10^{-6}$ atm
Mean free path	1.226 mm
Knudsen number	2.404×10^{-2}
Velocity	1720 m/s
Mach number	8.93
Axial density gradient	1.3%/mm

Results and Discussion

Results are presented for a free expansion flow of helium gas along a flat plate. The parameters describing the plate are presented in Table 2. The freestream conditions at the leading edge of the plate are presented in Table 3. The freestream Knudsen number based on the plate length is 2.404×10^{-2}; however, the local Knudsen numbers can be significantly larger as a result of the high temperatures within the thermal boundary layer.

Several computer runs have been made to study the dependence of the flowfield on the surface accommodation coefficients, leading edge bevel, and downstream boundary conditions. For the high resolution calculations presented here, the transverse dimension of each computational cell varies from one-half to one-tenth of the local mean free path as a result of variations in the flowfield gas density, whereas the axial dimension of each computational cell is always less than the local mean free path. The dependence of the computational accuracy on the Kn_c is discussed later.

Figure 2 presents an isodensity map for the flowfield above the plate surface. On can observe that an oblique shock propagates downstream from the plate leading edge. One can also observe significant upstream backscattering of molecules near the plate leading edge as a result of the flow rarefaction.

Figures 3 to 5 present several sets of comparisons between experimental data[2] and computational results for density, axial velocity, average translational temperature, and the average of

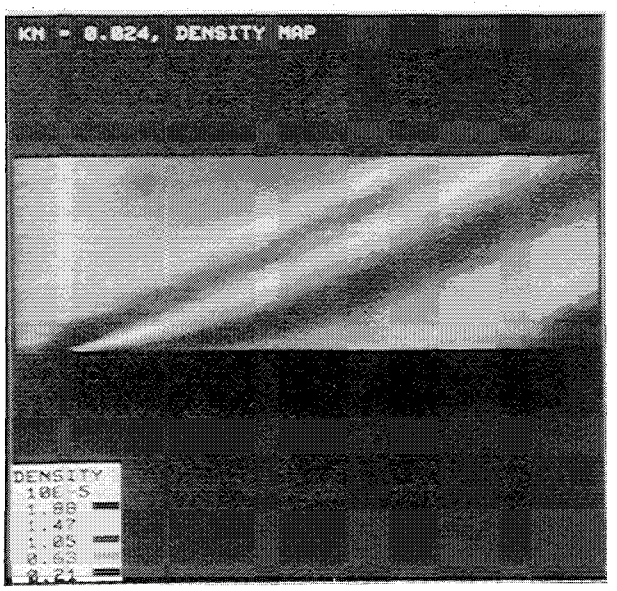

Fig. 2 Density map of flowfield above plate surface. Leading edge bevel is not represented.

the axial and surface normal components of the translational temperature. Each figure contains results for axial positions ranging from the plate leading edge to a position 31.5 mm downstream of the leading edge. The symbols represent the experimental data; the curves represent the computations. Transverse positions are normalized by the plate length; density and velocity are normalized by their respective freestream values at the leading edge; the temperatures are normalized by the flow stagnation temperature.

Figure 3 presents results for a flat plate without a leading edge bevel. Here, both the scattering angle and energy accommodation coefficients are set to unity. Figure 3a indicates excellent agreement between the computed density and the experimental measurements for all axial positions. One can observe a reduction in the gas density near the plate surface as a result of the viscous heating of the gas, which produces high transverse velocities of the surface-scattered molecules and a subsequent depletion of the gas from the surface region. The results also indicate peaks in the density profiles for each axial position. These peaks represent the formation of an oblique shock. Previous results[3] indicate that oblique shocks form at values of the $Kn_{\infty,L}$ less than 0.1. This is in agreement with the results presented here.

Figure 3b indicates that the velocity slip at the wall decreases with increasing axial distances as a result of the increasing number of molecular collisions with the wall. Comparisons of the computed results with the data indicate that for the upstream axial positions, the computed velocities exceed the measured velocities, whereas for the downstream axial positions the measured velocities exceed the computed velocities. These results imply that the accommodation coefficients used in the calculations are too small near the plate leading edge and too large at the downstream positions.

Figure 3c presents the average translational temperature, but Fig. 3d presents the average of only the axial and transverse components to allow comparison with what was actually measured. One can observe reductions in the temperature jumps at the wall with increasing axial positions, again, as a result of the increasing number of molecular collisions with increasing axial position. Comparison of the computed temperature results with the data indicates that, for reasons similar to those presented above in reference to the axial velocity, the accommodation coefficients used in the calculations are too small near the plate leading edge and too large at the downstream positions.

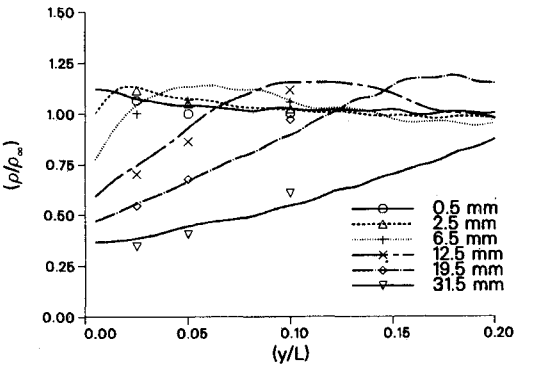

a) Density profiles normal to plate surface

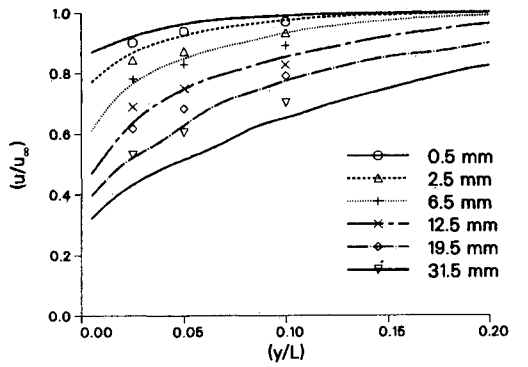

b) Axial velocity profiles normal to plate surface

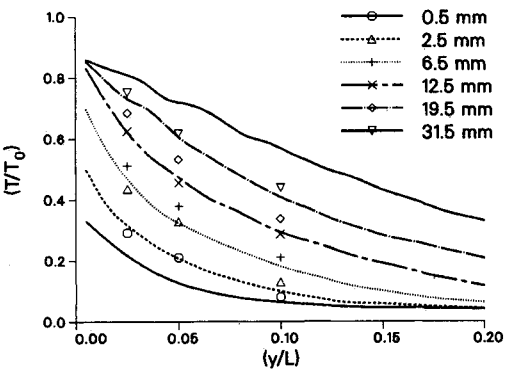

c) Mean temperature profiles normal to plate surface

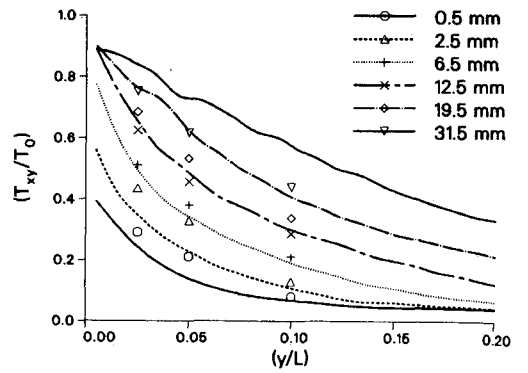

d) Two-component mean temperature profiles normal to plate surface

Fig. 3 Symbols represent data from Ref. 2; curves represent computations. Results presented for axial positions ranging from 0.5 mm to 31.5 mm from leading edge. Full surface accommodation and zero plate thickness are assumed.

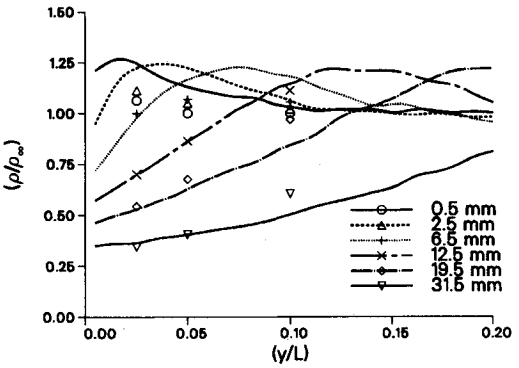

a) Density profiles normal to plate surface

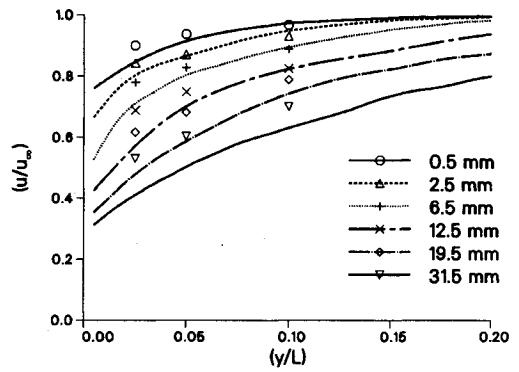

b) Axial velocity profiles normal to plate surface

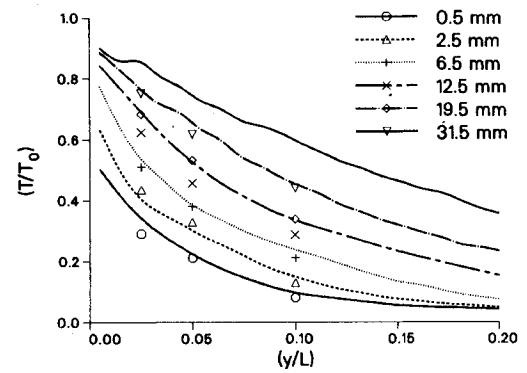

c) Mean temperature profiles normal to plate surface

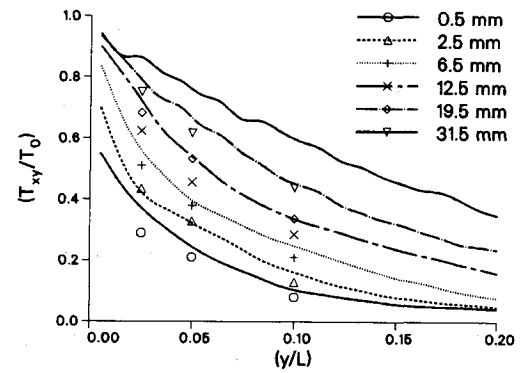

d) Two-component mean temperature profiles normal to plate surface

Fig. 4 Symbols represent data from Ref. 2; curves represent computations. Results presented for axial positions ragining from 0.5 mm to 31.5 mm from leading edge. Full surface accommodation, but a finite plate thickness of 6 mm and a leading edge bevel angle of 20 deg is used.

The need for larger accommodation coefficients for both the velocity and temperature profiles toward the leading edge, even though the surface scattering is fully accommodated and diffuse, implies that leading edge effects cannot be neglected. By accounting for the finite thickness of the plate and the leading edge bevel in the computations, the flux of molecules backscattered from the leading edge increases, and consequently, the apparent surface accommodation coefficients also increase.

Figure 4 presents a set of results similar to those in Fig. 3, except that a finite plate thickness of 6 mm with a 20 deg bevel angle are included to simulate the actual experimental configuration. Comparison of Fig. 4a with Fig. 3a indicates that inclusion of the leading edge effects has resulted in an overprediction of the leading edge density. However, the downstream density profiles are relatively unaffected. Comparison of the velocity and temperature profiles in Figs. 4b–4d with those of the previous set indicate that the inclusion of the leading edge effects now results in an overprediction of both the velocity and temperature accommodation coefficients for all axial positions.

Optimal agreement between measurement and computation is obtained when the leading edge effects are included and all the surface accommodation coefficients are reduced to 0.8. Figure 5a indicates good agreement between the computed and measured density profiles. There is approximately a 10% overprediction of the leading edge density. However, the downstream densities are in excellent agreement. Figures 5b–5d indicate that the computed velocity and temperature profiles are in good agreement with the measured values for all axial positions. Again, the largest discrepancies are towards the leading edge.

Additional computations were performed to study the dependence of the flowfield properties on various combinations of the accommodation coefficients. The results in Fig. 6 indicate that the flowfield is most sensitive to the scattering angle accommodation coefficient (AD), and least sensitive to the energy accommodation coefficient (AE). This can be attributed to the small difference between the flow stagnation temperature and surface temperature for the calculations presented here. Because the surface temperature is approximately equal to the flow stagnation temperature, the energy of a specularly reflected molecule is comparable to that of a molecule that thermally accommodates with the surface. Comparisons between the computations and the measurements in Fig. 6 indicate that, at both the leading edge and downstream positions, an accommodation coefficient between 0.5 and 1.0 would produce the best agreement. Results presented in the previous figure indicate that an accommodation coefficient of 0.8 provides optimal agreement between calculations and measurements. Comparisons between the measurements and continuum calculations are presented in Ref. 2 and suggest that the leading edge accommodation coefficients should be dramatically less than the values suggested here. However, as pointed out in Ref. 2, the continuum theory is not expected to produce accurate results in rarefied flows, such as exist here, particularly towards the plate leading edge.

Comparisons of the results for the free-flow downstream boundary condition with those for the zero axial gradient boundary condition[8] indicate no dependence of the flowfield on the downstream boundary condition. This can be attributed to the high axial Mach numbers at the exit boundary. The lowest exit plane Mach number is approximately 2.0 at a position adjacent to the plane of the plate surface. These results, therefore, indicate that for exit plane Mach numbers greater than or equal to 2.0, one need not be concerned with thermal influx of molecules through the downstream boundary.

Figure 7 compares the computed skin friction for values of the $Kn_{\infty,c}$ ranging from 2.452 to 0.1226. Here, the value of the $Kn_{\infty,c}$ is varied by varying the transverse cell size. The skin friction is computed by summing the axial momentum flux imparted to a wall segment as a result of molecular collisions

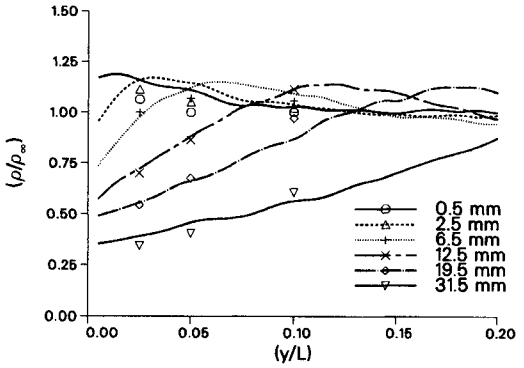

a) Density profiles normal to plate surface

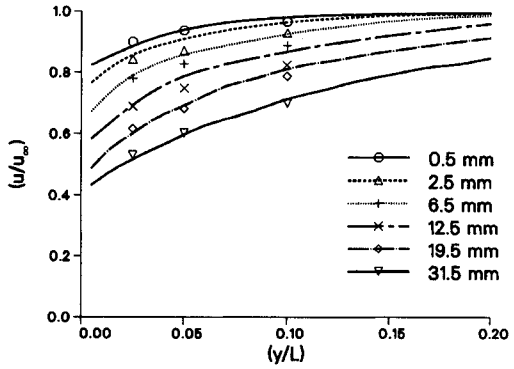

b) Axial velocity profiles normal to plate surface

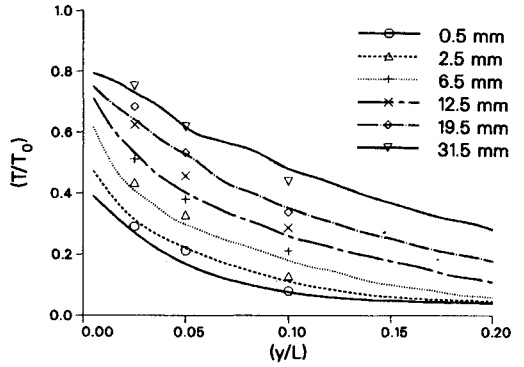

c) Mean temperature profiles normal to plate surface

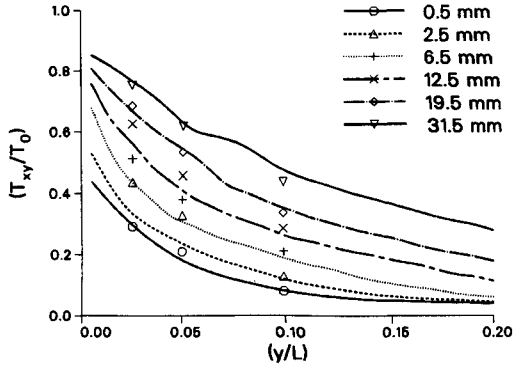

d) Two-component mean temperature profiles normal to plate surface

Fig. 5 Symbols represent data from Ref. 2; curves represent computations. Results presented for axial positions ranging from 0.5 mm to 31.5 mm from leading edge. Surface accommodation coefficients for translational energy and scattering angle are set to 0.8. Plate thickness is 6 mm and the leading edge bevel angle is 20 deg.

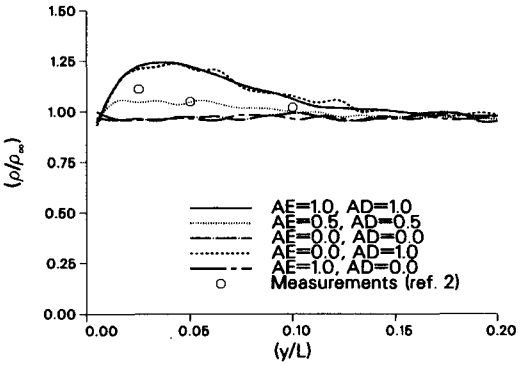

a) Computed and measured density profiles at an axial position of 2.5 mm

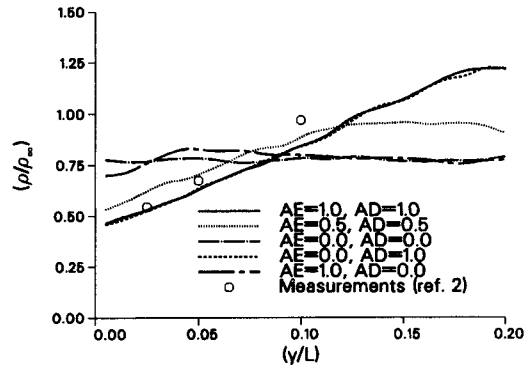

b) Computed and measured density profiles at an axial position of 19.5 mm

Fig. 6 Computations performed for several energy (AE) and scattering (AD) accomodation coefficients.

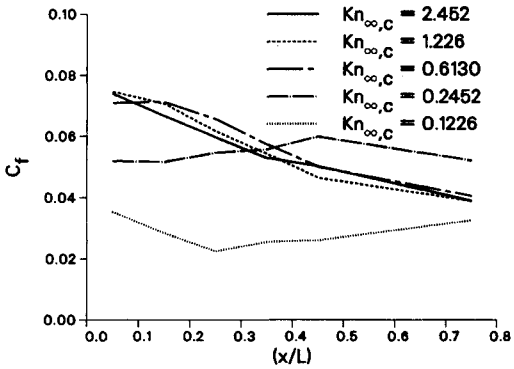

Fig. 7 Computed skin friction vs axial position along the plate. Results are presented for five mesh resolutions corresponding to freestream Knudsen numbers based on cell size ranging from 2.452 to 0.1226.

with the segment. Consequently, the computed skin friction for each segment represents an average value for that segment. The surface is divided into six segments. The first five segments are equal in length and cover the leading half of the plate. The sixth segment is the trailing half of the plate. The skin friction value for each segment is plotted vs the axial position of the center of the corresponding segment.

The results in Fig. 7 indicate that the skin friction is insensitive to the $Kn_{\infty,c}$ for values of the Knudsen number greater than 0.613. This implies that a transverse cell size comparable in magnitude to the local mean free path is adequate for accurate predictions of skin friction. Detailed comparisons of the flowfield densities, velocities, and temperatures indicate that

these results are also insensitive to the $Kn_{\infty,c}$ for values of the Knudsen number greater than 0.613. However, for values of the $Kn_{\infty,c}$ less than 0.613, the skin friction is underpredicted at the upstream axial positions. Examination of the detailed flowfield properties indicates that this results from an underprediction of the transverse flux of axial momentum towards the surface. At axial positions further downstream, corresponding to more continuum flow, preliminary results indicate that a coarse mesh overpredicts the skin friction. This can be attributed to an overprediction of the gas viscosity. When the cell size in the direction of the macroscopic gradients exceeds the molecular mean free path, then the cell size replaces the mean free path as the effective length scale over which the molecular properties, such as momentum, are exchanged. Consequently, in the continuum limit, where even the coarse mesh flowfield has had sufficient surface collisions to accommodate with the surface, the coarse mesh may overpredict the gas viscosity and corresponding skin friction.

Conclusions

Results have been obtained using the direct simulation Monte Carlo technique for the diverging flow of helium gas along a flat plate. The results compare favorably with available data,[2] when one accounts for the finite plate thickness and leading edge bevel angle, in addition to accounting for partial accommodation at the plate surface. An overall accommodation coefficient of 0.8 gives the best agreement with the experimental data.[2] The results are found to be insensitive to the accommodation coefficient for the translational energy because the flow stagnation and surface temperatures are comparable in magnitude.

Examination of two downstream boundary conditions, an unconstrained outflow condition and a zero axial gradient condition, indicate no dependence of the flowfield within the domain on the downstream boundary condition for exit plane Mach numbers greater than or equal to 2.0.

Skin friction results are presented for a variety of transverse mesh resolutions corresponding to values of the $Kn_{\infty,c}$, ranging from 2.452 to 0.1226. These results, in conjunction with flowfield results, indicate that for values of the $Kn_{\infty,c}$ that are greater than unity, corresponding to values of the Kn_c that are also greater than unity, the computed skin friction and corresponding flowfield properties are insensitive to the mesh resolution. However, for values of the $Kn_{\infty,c}$ less than unity, the skin friction is underpredicted at upstream positions and overpredicted at downstream positions.

Acknowledgments

The work represented in this paper was supported by the U.S. Department of Energy. The author greatly appreciates the assistance of Dr. Robert Cattolica in the interpretation of the experimental data in Ref. 2, with which the computations were compared.

References

[1]Bird, G. A., *Molecular Gas Dynamics*, Clarendon Press, Oxford, 1976.

[2]Becker, M., Robben, F., and Cattolica, R., "Velocity Distribution Fucntions Near the Leading Edge of a Flat Plate," *AIAA Journal*, Vol. 12, Sept. 1974.

[3]Hermina, W. L., "Monte Carlo Simulation of Transitional Flow Around Simple Shaped Bodies," *Proceedings of the 15th International Symposium on Rarefied Gas Dynamics*, Vol. 1, edited by V. Boffi and C. Gercignani, B. G. Teubner, Stuttgart, 1986, pp. 452–460.

[4]Hermina, W. L., "Monte Carlo Simulation of Rocket Plume Enhancement Regions," 15th JANNAF Plume Technology Meeting. Fort Sam Houston, San Antonio, TX, May 21–23, 1985.

[5]Hermina, W. L., "Monte Carlo Simulation of High-Altitude Rocket Plumes with Nonequilibrium Molecular Energy Exchange," AIAA Paper 86-1318, June 1986.

[6]Bird, G. A., "Monte Carlo Simulation in an Engineering Context," *Progress in Astronautics and Aeronautics: Rarefied Gas Dynamics Part I*, Vol. 74, edited by Sam S. Fisher, AIAA, New York, 1980, p. 239.

[7]Chapman, S. and Cowling, T. G., *The Mathematical Theory of Non-Uniform Gases*, Cambridge University Press, Cambridge, 1970.

[8]Vogenitz, F. W., Broadwell, J. E., and Bird, G. A., "Leading Edge Flow by the Monte Carlo Direct Simulation Technique," *AIAA Journal*, Vol. 8, March 1970.